RSC Advances

PAPER

View Article Online
View Journal | View Issue

Check for updates

Cite this: *RSC Adv.*, 2025, **15**, 30817

# Efficient peroxymonosulfate activation by magnesium-doped $Co_3O_4$ for thiacloprid degradation: regulation of $Co^{2+}/Co^{3+}$ ratios and degradation mechanism

Hui Fui, *[ab] Xinran Ma,[b] Yiping Huang,[b] Shiyao Xi,[b] Zhandong Ren[ab] and Yuchan Zhu[ab]

AS a low-cost and high-performance catalyst, spinel cobalt oxide ($Co_3O_4$) has two different catalytic active sites (tetrahedral $Co^{2+}$ and octahedral $Co^{3+}$) to drive the activation of peroxymonosulfate (PMS) through $Co^{2+}/Co^{3+}$ redox cycle. Tuning $Co^{2+}/Co^{3+}$ atomic ratio on the surface of $Co_3O_4$ for the construction of a synergy in the $Co^{2+}/Co^{3+}$ redox cycle might be an effective way to further boost PMS activation performance of $Co_3O_4$ catalyst. Herein, we suggested a metal-doping strategy to regulate $Co^{2+}/Co^{3+}$ atomic ratio of $Co_3O_4$ by partially substituting $Co^{2+}$ with inert $Mg^{2+}$ and formed a series of Mg doped $Co_3O_4$ (MCO) catalysts. Structural characterizations and experimental investigations demonstrated that Mg doping did not change $Co_3O_4$ host lattice and particle morphology, but could manipulate surface $Co^{2+}/Co^{3+}$ atomic ratio of $Co_3O_4$ for an improved PMS activation. The optimal MCO catalysts (MCO-0.2) with the suitable $Co^{2+}/Co^{3+}$ atomic ratios (1.13) exhibited the excellent thiacloprid (THIA) degradation performance through PMS activation, and the apparent degradation rate constant (0.2835 $min^{-1}$) was highly outperformed that of pure $Co_3O_4$ (0.09555 $min^{-1}$) and other similar cobalt-based catalysts. The optimal THIA degradation conditions might be: catalyst dose 100 mg $L^{-1}$, PMS concentration 0.8 mM, pH 7 and THIA concentration 20 mg $L^{-1}$. Quenching experiments and electron paramagnetic resonance (EPR) characterizations suggested $SO_4^{\bullet-}$, $HO^{\bullet}$ and $^1O_2$ were all involved in THIA degradation during the MCO-0.2/PMS process. Furthermore, the steady-state concentrations of these reactive species and their relative contributions to THIA degradation were also calculated by combining a kinetic model and a series of probe compound-based experiments. The results indicated that $SO_4^{\bullet-}$ and $HO^{\bullet}$ were generated at lower steady-state concentrations than that of $^1O_2$, but they dominated THIA abatement during the MCO-0.2/PMS process. This study presented new insights into the construction of efficient PMS activator and a mechanistic understanding for PMS-mediated reaction.

Open Access Article. Published on 28 August 2025. Downloaded on 2/6/2026 8:32:13 AM.
This article is licensed under a Creative Commons Attribution 3.0 Unported Licence.

Received 10th June 2025
Accepted 21st August 2025

DOI: 10.1039/d5ra04080a

rsc.li/rsc-advances

## 1. Introduction

Refractory organic pollutants (*e.g.*, pesticides, antibiotics and industrial chemicals) in wastewater constitute a serious threat to the ecosystem and human health.[1–3] For eliminating these organic pollutants from wastewater, peroxymonosulfate-based advanced oxidation processes (PMS-AOPs) have been extensively studied and recognized as a promising approach[4–6] during the past few years. In PMS-AOPs, reactive species (RS) originated from PMS activation is crucial to accelerate these organic pollutants degradation.[7–9] Therefore, many catalysts, including some transition metals (Co, Fe, Cu and Mn),[10–13] carbonaceous materials and their composites,[14,15] have been developed for efficient PMS activation during the past few years. Of all these catalysts, Co-based heterogeneous catalysts (*e.g.*, metal ions, oxides, hydroxides and Co-containing single atomic catalysts)[16–20] have drawn extensive attention because they are amongst the most active PMS activator and can be recycled to minimize environmental impact.[21,22]

Among various Co-based catalysts, $Co_3O_4$ stands out as a low-cost catalyst and was widely used in different oxidation reaction systems.[23,24] Normal $Co_3O_4$ catalysts with two different Co sites in a spinel structure, where $Co^{2+}$ is bonded to four neighboring oxygen atoms at tetrahedral sites and $Co^{3+}$ is bonded to six neighboring oxygen atoms at the octahedral sites, have been demonstrated to be efficient for PMS activation.[25,26] Previous studies[27,28] have revealed that both tetrahedral $Co^{2+}$ and octahedral $Co^{3+}$ were the efficient active sites of PMS activation in PMS-AOPs over the $Co_3O_4$ catalysts. Specifically, two

[a]*Hubei Province Key Laboratory of Agricultural Waste Resource Utilization, Wuhan Polytechnic University, Wuhan 430023, China. E-mail: feihui509@163.com*
[b]*School of Chemistry and Environmental Engineering, Wuhan Polytechnic University, Wuhan 430023, China*

© 2025 The Author(s). Published by the Royal Society of Chemistry

Open Access Article. Published on 28 August 2025. Downloaded on 2/6/2026 8:32:13 AM. This article is licensed under a Creative Commons Attribution 3.0 Unported Licence.

reactions (the reductive reaction of PMS and the oxidative reaction of PMS) should take place simultaneously to generate radicals continuously through a $Co^{2+}/Co^{3+}$ redox cycle (eqn (1) and (2)).[27,28]

The oxidative reaction of PMS:

$$Co^{2+} + HSO_5^- \rightarrow Co^{3+} + SO_4^{\cdot -} + OH^- \quad (1)$$

The reductive reaction of PMS:

$$Co^{3+} + HSO_5^- \rightarrow Co^{2+} + SO_5^{\cdot -} + H^+ \quad (2)$$

Undoubtedly, the different density of $Co^{2+}/Co^{3+}$ on the surface of $Co_3O_4$ catalysts might be resulted in the different capacity for the circulation of $Co^{2+}/Co^{3+}$ and further vigorously affect the activity of $Co_3O_4$ catalysts.[29] Moreover, the different density of $Co^{2+}/Co^{3+}$ on the surface could also change atomic arrangements and electronic structures of $Co_3O_4$ to favour $Co^{2+}/Co^{3+}$ redox cycle.[30,31] Thus, tuning the atomic ratios of $Co^{2+}/Co^{3+}$ exposed on the surface of $Co_3O_4$-based catalytic materials could be a reasonable way to construct a synergistic effect of $Co^{2+}$ and $Co^{3+}$ in the $Co^{2+}/Co^{3+}$ redox cycle for an improved PMS activation.

Metal doping was a simple and efficient approach to engineer surface tetrahedral $Co^{2+}$ and octahedral $Co^{3+}$ of $Co_3O_4$ for manipulating the ratio of $Co^{2+}/Co^{3+}$ of $Co_3O_4$ by the substitution of tetrahedral $Co^{2+}$ and octahedral $Co^{3+}$ with the corresponding valence states of inactive metal.[32,33] For example, Dong's group[17] reported the synthesis of Al doped $Co_3O_4$ catalysts by incorporating inert $Al^{3+}$ ion into the lattice of $Co_3O_4$. They found that Al incorporation could partly replace octahedral $Co^{3+}$ and modify the ratio of $Co^{2+}/Co^{3+}$ in $Co_3O_4$ for an improved performance of PMS activation. While previous studies[34] have demonstrated octahedral $Co^{3+}$ possessed a high standard reduction potential ($E_0(Co^{3+}/Co^{2+})$ = 1.92 V) and was notably more active than tetrahedral $Co^{2+}$ for OER. The significant roles for pollutant abatement of octahedral $Co^{3+}$ were also confirmed during the PMS-AOPs.[35] Therefore, the engineering of tetrahedral $Co^{2+}$ by the doping of divalent metal ion ($Zn^{2+}$ and $Mg^{2+}$) might be an effective way to regulate the atomic ratio of $Co^{2+}/Co^{3+}$ of $Co_3O_4$ for an improved PMS activation.[10,20] While $Mg^{2+}$ has a similar ionic radius to that of $Co^{2+}$ (0.72 Å *vs.* 0.74 Å).[28] The precise substitution of tetrahedral $Co^{2+}$ with inert $Mg^2$ could be easily realized for the regulation of $Co^{2+}/Co^{3+}$ ratio in the spinel structure of $Co_3O_4$, but might not change $Co_3O_4$ host lattice,[28,29] which facilitated us to judge the important role of $Co^{2+}/Co^{3+}$ ratio in PMS activation, however it has not been reported yet.

Hence, a magnesium doping strategy was developed to manipulate $Co^{2+}/Co^{3+}$ ratio in the cobalt spinel for an enhanced PMS activation, and obtained a series of Mg doped $Co_3O_4$ (MCO) catalysts. Optimal MCO catalysts (MCO-0.2) with suitable $Co^{2+}/Co^{3+}$ atomic ratios possessed superior activities for THIA degradation during PMS-AOPs, and the rate constant (0.2835 $min^{-1}$) was 2.97 folds faster than that of pure $Co_3O_4$ (0.0955 $min^{-1}$). To further elucidate the degradation mechanisms, the formation of reactive species in the MCO-0.2/PMS process was verified by scavenger tests and EPR characterizations. Moreover, the steady-state concentrations of these RS were quantified through a kinetic model and several probe experiments. Using the newly measured kinetic data, the relative contributions of these RS to THIA degradation were thus determined. This study might present valuable design guide of cobalt-based catalysts with regulated $Co^{2+}/Co^{3+}$ ratio for environmental applications.

## 2. Experimental procedures

### 2.1. Chemicals and materials

Thiacloprid (THIA), sodium hydroxide (NaOH), atrazine (ATZ), cobalt nitrate hexahydrate ($Co(NO_3)_2 \cdot 6H_2O$), sodium bicarbonate ($NaHCO_3$), methanol (MeOH), magnesium nitrate dihydrate ($Mg(NO_3)_2 \cdot 2H_2O$), chloramphenicol (CAP) and *tert*-butyl alcohol (TBA) were obtained from Sinopharm Chemical Reagent Co. Ltd. Potassium peroxymonosulfate (PMS), sodium chloride (NaCl), sulfuric acid ($H_2SO_4$), sodium nitrate ($NaNO_3$), disodium hydrogen phosphate ($Na_2HPO_4$), sodium thiosulfate ($Na_2S_2O_3$), furfuryl alcohol (FFA), methyl phenyl sulfone ($PMSO_2$), metronidazole (MTZ), methyl phenyl sulfoxide (PMSO), commercial nano-$Co_3O_4$ and $MgCo_2O_4$ were purchased from Aladdin Company, China. All chemical reagents were used without further purification. Deionized water (DI water) was used throughout the whole experiments.

### 2.2. Catalyst synthesis

The synthesis of MCO catalysts involved the pre-synthesis of Co-based precursors and subsequently calcining them under air atmosphere. The obtained catalysts were labelled MCO-*X*, where *X* indicated the nominal molar ratio of Mg/(Co + Mg) in the catalysts. Taking MCO-0.2 as an example, 1.5 mmol $Mg(NO_3)_2 \cdot 2H_2O$ and 6 mmol $Co(NO_3)_2 \cdot 6H_2O$ were mixed in 100 mL DI water. Subsequently, the solution pH was adjusted to 11 by dropwise addition of 0.1 M NaOH solution under continuous stirring. The above solution was centrifugated at 10 000 rpm for 10 min, and the obtained precipitate was resuspended in a small volume of DI water, repeating the procedure until the suspension pH reached 8. After rinsing with ethanol several times, the precipitate was dried at 80 °C for 24 h, and then thermally treated at 350 °C for 3 h in air atmosphere to obtain the final product. Similarly, $Co_3O_4$ ($Co(NO_3)_2 \cdot 6H_2O$: 7.5 mmol), MCO-0.1 ($Mg(NO_3)_2 \cdot 2H_2O$: 0.75 mmol, $Co(NO_3)_2 \cdot 6H_2O$: 6.75 mmol), MCO-0.3 ($Mg(NO_3)_2 \cdot 2H_2O$: 2.25 mmol, $Co(NO_3)_2 \cdot 6H_2O$: 5.25 mmol) were prepared as above using different doses of $Mg(NO_3)_2 \cdot 2H_2O$ and $Co(NO_3)_2 \cdot 6H_2O$. For comparison, $ZnCo_2O_4$ was prepared through the above procedure with appropriate doses of $Zn(NO_3)_2 \cdot 2H_2O$ and $Co(NO_3)_2 \cdot 6H_2O$. β-$Co(OH)_2$ were synthesized with same method as that of $Co_3O_4$ without thermal treatment.

### 2.3. Catalytic performance

The activities of $Co_3O_4$ and MCO catalysts were checked in 100 mL THIA solution with mechanically agitating. Specifically, the catalysts were first spiked into THIA solution and further stirred until adsorption/desorption equilibrium, followed by


© 2025 The Author(s). Published by the Royal Society of Chemistry

Open Access Article. Published on 28 August 2025. Downloaded on 2/6/2026 8:32:13 AM. This article is licensed under a Creative Commons Attribution 3.0 Unported Licence.

the initiation of the reaction with the introduction of 0.2 mM PMS. Periodically, 2 mL samples were filtered through a 0.22 μm filter and immediately quenched with $Na_2S_2O_3$ solution, followed by component analysis. The pH value of the reaction system was under control utilizing 0.1 M NaOH or $H_2SO_4$. The presence of reactive species (RS) in THIA degradation was evaluated by scavenger tests, where TBA, MeOH, DMSO and FFA were used as RS quenchers and spiked into the system before PMS addition. In addition, the depletion experiments of several probe compounds (including CAP, ATZ and MTZ) were performed as the same conditions as that of THIA abatement to measure RS exposures during the MCO-0.2/PMS process. Moreover, the reusability of MCO-0.2 catalysts was investigated through recycle tests. After each run, MCO-0.2 water and then reused under the same experimental conditions (details provided in Text S1).

### 2.4. Analytical methods

The crystalline structures of the synthetized catalysts were detected by a Bruker D8 Advance X-ray diffractometer (XRD) using Cu Ka radiation ($\lambda = 1.5418$ Å) with 2-theta range of 10–80° and scanning rate of 10° $s^{-1}$. The micro-morphologies of pure $Co_3O_4$ and MCO-0.2 catalysts were measured by scanning electron microscope (SEM, Zeiss Gemini 300) equipped with energy dispersive spectrometer (EDS, Oxford X-MAX). The surface elements and chemical valences of pure $Co_3O_4$, MCO-0.1 and MCO-0.2 catalysts were analysed by X-ray photoelectron spectroscopy (XPS, Thermo Scientific ESCALAB 250, USA) with Al Ka radiation, and the binding energies were calibrated with the residual C 1s peak (284.8 eV). Zeta potentials of MCO-0.2 catalysts were measured by Malvern Zeta sizer Nano ZS90 through the method described in Text S2. Electron paramagnetic resonance (EPR) signals of active species were monitored on a Bruker A300 EPR spectrometer using TEMP or DMPO as capture agents. In addition, the concentration of THIA and probe compounds were determined by high-performance liquid chromatography (HPLC, Agilent 1260), and the details of the measurements were illustrated in Text S3. Cobalt dissolution amount was measured by inductively coupled plasma-mass spectrometry (ICP-MS, Optima 5300 DV, USA). The residual concentrations of PMS were analyzed through the method described in Text S4.

## 3. Results and discussion

### 3.1. Characterization of MCO catalysts

MCO catalysts were prepared through a co-precipitation method followed by the calcination in air (Fig. 1a), in which the precipitate was recovered by the centrifugation at 10 000 rpm and then resuspended in DI water, repeating the sequence several times to obtain the mono-dispersed catalysts. By adjusting the amounts of Mg ions in the precursor, the Mg doping degree could be controlled and a series of MCO catalysts were obtained. SEM images of $Co_3O_4$ and MCO-0.2 catalysts were presented in Fig. 1b and c, suggesting $Co_3O_4$ exhibited the granular structure with an average diameter around 40 nm. Notably, MCO-0.2 exhibited a similar size and shape to that of $Co_3O_4$, which indicated that Mg doping did not destroy the sample morphology. Moreover, EDS analysis (Fig. 1d and e) demonstrated the presence of Co, O and Mg elements in MCO-0.2, and Mg/Co atomic ratio was about 1 : 23, suggesting partial Co could be substituted by Mg atoms. These results suggested that MCO catalysts with similar morphology and different Mg contents were successfully synthesised, which facilitate us to judge the important role of Mg doping in PMS activation.

XRD measurements were employed to verify the crystal characteristics of $Co_3O_4$ and MCO-*X* catalysts. As can be seen in Fig. 2a, XRD pattern of $Co_3O_4$ exhibited the diffraction peaks at $2\theta$ values of 18.9°, 31.3°, 36.9°, 38.4°, 44.8°, 55.7°, 59.2°, and 65.2° were attributed to (111), (220), (311), (222), (400), (422), (511) and (440) lattice planes of the spinel-type $Co_3O_4$ (space group $Fd\bar{3}m$, JCPDS card no. 42-1467).[9,13] For MCO catalysts, only peaks of $Co_3O_4$ can be observed, indicating that Mg atoms should incorporate into the $Co_3O_4$ crystal lattice and the introduction of Mg did not change the $Co_3O_4$ host lattice, due to similar ionic radius of $Mg^{2+}$ to that of $Co^{2+}$ (0.72 Å of $Mg^{2+}$ *vs.* 0.74 Å of $Co^{2+}$).[17,28] After all, $Mg^{2+}$ has a little smaller ionic radius to that of $Co^{2+}$, Mg doping might lead to a slight change of peak positions and intensities for these catalysts.[28,29] Specially, a slight shift of the peak representing the (311) plane to lower angle can be observed by expanding the abscissa (Fig. 2b) of the XRD patterns for the MCO-*X* catalysts in comparison with that of the pure $Co_3O_4$. Since the (311) lattice plane of $MgCo_2O_4$ is lower to that of $Co_3O_4$ by about $2\theta = 0.047°$,[13] the shift should be caused by the substitution of tetrahedral $Co^{2+}$ with $Mg^{2+}$. As Mg/Co atomic ratio increased, a further shift to the lower angle appeared on the series of MCO-*X* catalysts, indicating more tetrahedral $Co^{2+}$ could be substituted by $Mg^{2+}$. This structure change might lead to the improved chemical properties and the higher activity.[13]

XPS analysis was performed to probe surface elements and chemical states of pure $Co_3O_4$, MCO-0.1 and MCO-0.2 catalysts. The survey spectra (Fig. 2c) clearly confirmed the presence of Co, O and Mg elements in MCO-0.1 and MCO-0.2 catalysts, and the corresponding Mg 2p spectra (Fig. 2d) exhibited a characteristic peaks of Mg 2p, testifying the Mg atoms might be incorporated into the crystal structure of $Co_3O_4$, which agreed well with XRD measurements. In the Co 2p spectra (Fig. 2e), two main peaks at 779.4 and 794.5 eV should be attributed to Co $2p_{3/2}$ and Co $2p_{1/2}$, respectively, along with their corresponding satellite peaks (denoted as "sat.") at 788.1 and 803.1 eV. The Co $2p_{3/2}$ spectra were fitted into $Co^{2+}$ and $Co^{3+}$ constituents at 779.7 and 781 eV, while Co $2p_{1/2}$ were also separated into the same components at 725.8 and 727.45 eV respectively.[36,37] The ratio of their fitted peak area revealed that $Co^{2+}/Co^{3+}$ atomic ratio gradually decreased with the increment of Mg content, verifying Mg doping could be a potential strategy for manipulating surface metal state of $Co_3O_4$ toward improved activities. Meanwhile, the O 1s spectra (Fig. 2f) displayed three peaks, which ascribed to lattice oxygen ($O_L$, ~529.5 eV), surface hydroxyl groups ($O_{OH}$, ~530.3 eV), and oxygen vacancies ($O_v$, ~531.6 eV).[38] Notably, the peak area ratio of deficient oxygen gradually increased with increased Mg content, confirming Mg

Open Access Article. Published on 28 August 2025. Downloaded on 2/6/2026 8:32:13 AM.
This article is licensed under a Creative Commons Attribution 3.0 Unported Licence.

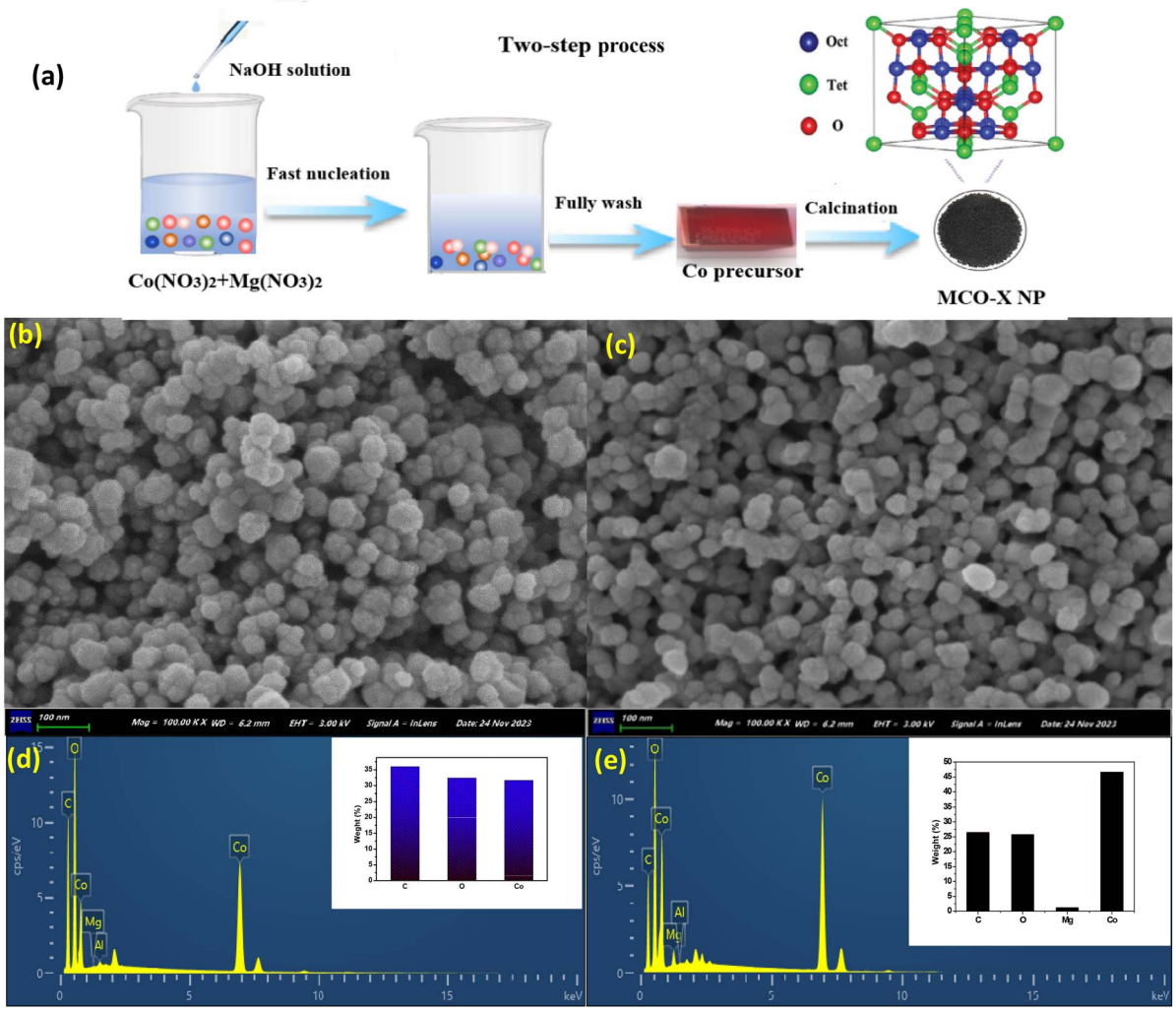


Fig. 1 (a) Schematic illustration of the preparation of MCO-*X* catalysts, SEM images of (b) $Co_3O_4$ and (c) MCO-0.2; EDS spectra for (d) $Co_3O_4$ and (e) MCO-0.2, respectively.

doping might create new oxygen vacancies.[39] The finding revealed that due to the lower $Co^{2+}/Co^{3+}$ atomic ratio induced by Mg doping, the neighbouring oxygen atom might be more easily oxidized by octahedral $Co^{3+}$ and squeezed out of the crystalline structure, thus forming MCO-0.2 with enriched oxygen vacancies at the surface.[40]

### 3.2. Catalytic activity of MCO catalysts

The catalytic activities of MCO catalysts were evaluated in thiacloprid (THIA) degradation *via* PMS activation. Fig. 3a showed negligible THIA removal was observed when each catalyst or PMS was used separately. Optimization experiments for the catalysts were also determined. Fig. 3b showed a volcano-like relationship between the catalytic performance and Mg doping amount. MCO-0.2 exhibited the best catalytic performance for THIA degradation and the rate constants was 0.28347 $min^{-1}$, which was about 2.97, 2.02 and 1.35 times higher than that of $Co_3O_4$ (0.09555 $min^{-1}$), MCO-0.1 (0.14045 $min^{-1}$) and MCO-0.3 (0.20932 $min^{-1}$), respectively. On the other hand, PMS decomposition (Fig. 3d and e) on the surface of different catalyst was in line with THIA degradation, which could be attributed to the fact that the catalyst accelerated the PMS activation to produce more ROS, thus resulting in significant THIA degradation. The depletion rates constants of PMS in MCO-0.3, MCO-0.2, MCO-0.1 and $Co_3O_4$ systems were 0.02597, 0.03648, 0.01145 and 0.01447 $min^{-1}$, respectively. The above results suggested the important function of Mg doping in tuning the $Co^{2+}/Co^{3+}$ ratio for enhanced THIA degradation. MCO-0.2 might have the rational $Co^{2+}/Co^{3+}$ ratio, which facilitate the $Co^{2+}/Co^{3+}$ recycle, thus promoting PMS activation toward a significantly improved THIA degradation. However, the excessive substitution of $Co^{2+}$ with Mg in MgCO-0.3 might deteriorating the $Co^{2+}/Co^{3+}$ recycle, ultimately resulting in the decrease of degradation efficiency.[17]

To further verify the excellent activation performance of MCO-0.2 catalyst toward PMS, Similar catalysts such as β-$Co(OH)_2$ and $ZnCo_2O_4$ were used to activate PMS for THIA degradation. As reported,[35,41] the majority of cobalt was $Co^{2+}$ ions at the tetrahedral sites of β-$Co(OH)_2$, while most of cobalt


© 2025 The Author(s). Published by the Royal Society of Chemistry

Open Access Article. Published on 28 August 2025. Downloaded on 2/6/2026 8:32:13 AM.
This article is licensed under a Creative Commons Attribution 3.0 Unported Licence.

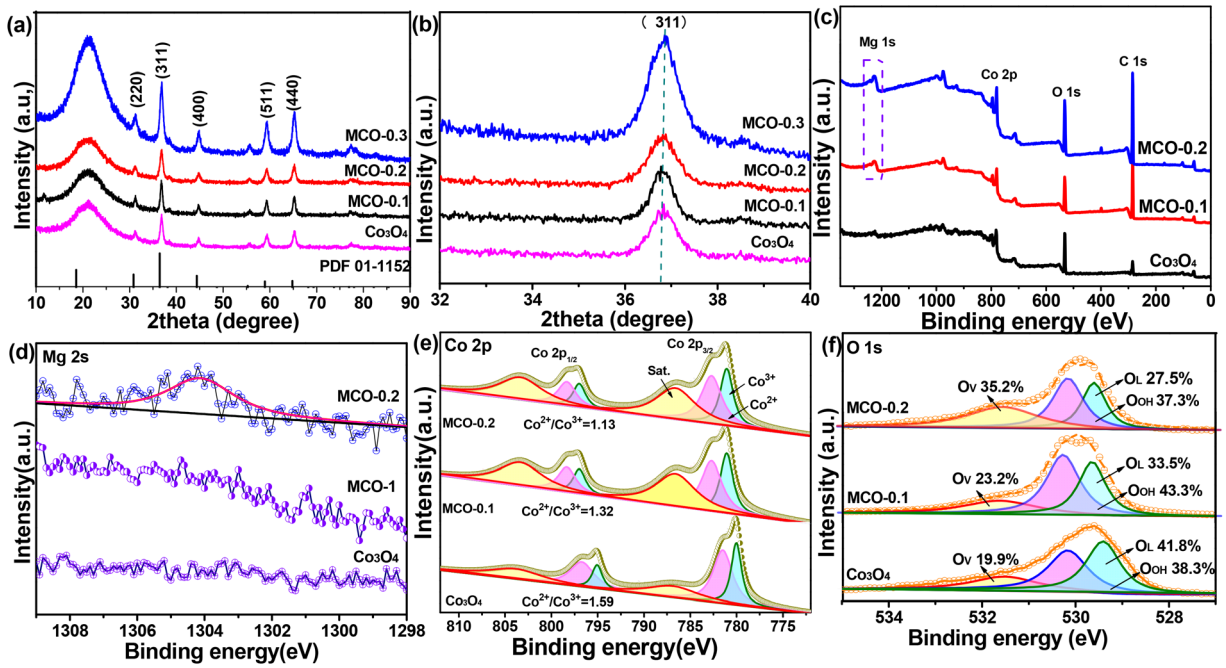


Fig. 2 (a) XRD patterns and (b) the diffraction peak at 36–37.5° expanded in the abscissa; (c) XPS survey spectra, high-resolution XPS spectra of (d) Mg 2s, (e) Co 2p, (f) O 1s of $Co_3O_4$, MCO-0.1 and MCO-0.2 catalysts, respectively.

was $Co^{3+}$ ions at the octahedral sites of $ZnCo_2O_4$. Under the same conditions, the activation performance of these two catalysts (Fig. 3c and S1c) was considerably lower than that of MCO-0.2, with THIA removals of 78.7.2% and 48.2%, respectively, which suggested that the rational $Co^{2+}/Co^{3+}$ ratio in MCO-0.2 catalysts could favour $Co^{2+}/Co^{3+}$ recycle and boost the PMS activation toward a rapid THIA degradation. Furthermore, in comparison with commercial $Co_3O_4$ (denoted as C-$Co_3O_4$) and $MgCo_2O_4$ under the identical conditions (Fig. 3c and S1c), it was observed that the MCO-0.2 exhibited the higher THIA removal rates, which also highly outperformed many other reported cobalt-based catalysts (Table S2), indicating that MCO-0.2 had

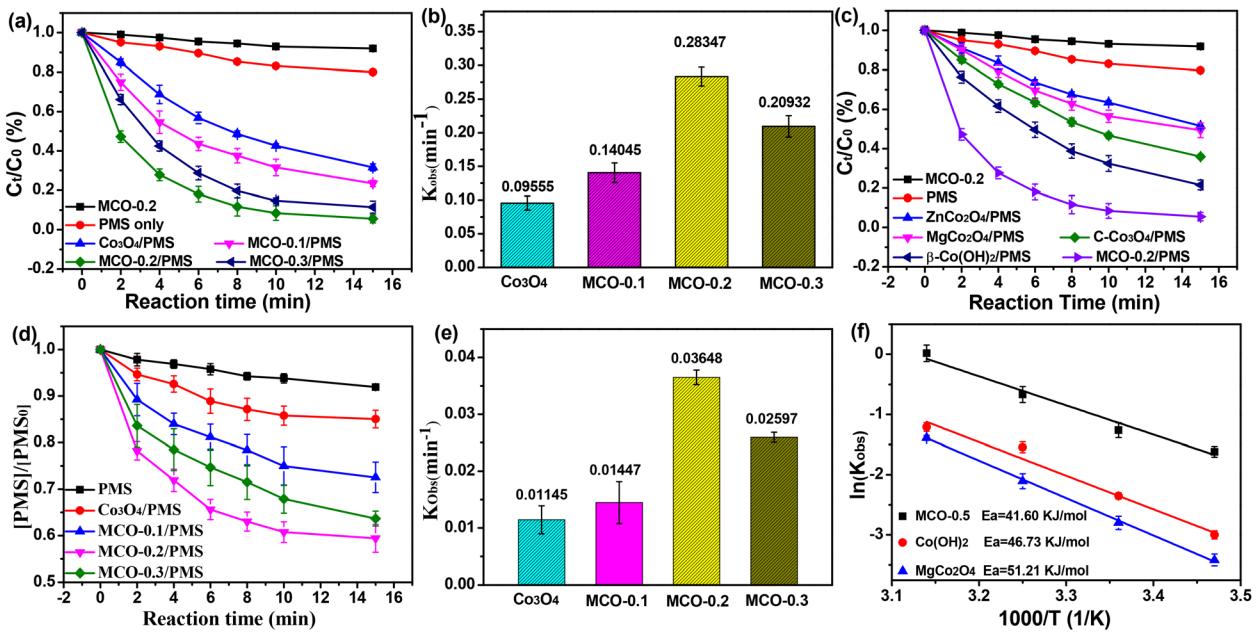


Fig. 3 (a) THIA removal and (d) PMS depletion over $Co_3O_4$ and MCO-*X* catalysts, (b) and (e) the corresponding first-order rate constants; (c) THIA removal curves over MCO-0.2 and other similar catalysts, (f) the corresponding Arrhenius plots. Experiment conditions: pH = 7, [THIA] = 20 mg $L^{-1}$, [catalyst] = 100 mg $L^{-1}$, [PMS] = 0.4 mM.

Open Access Article. Published on 28 August 2025. Downloaded on 2/6/2026 8:32:13 AM.
This article is licensed under a Creative Commons Attribution 3.0 Unported Licence.

the extremely superior ability of PMS activation and great application potential. More interestingly, the activation energies ($E_a$) derived from a series of kinetic experiments also exhibited the similar trend (Fig. 3f and S2). The activation energy ($E_a$) of the MCO-0.2/PMS system was calculated to 41.6 kJ mol$^{-1}$ through Arrhenius formula, which was considerably lower than that of $Co(OH)_2$/PMS (46.7 kJ mol$^{-1}$) and $ZnCo_2O_4$/PMS (51.2 kJ mol$^{-1}$) systems, indicating that the rational $Co^{2+}/Co^{3+}$ ratio in MCO-0.2 catalyst could notably promote THIA degradation by lowering $E_a$. Thus, we selected MCO-0.2, which displayed the superior PMS activation capability, as the catalyst for further experiments.

### 3.3. Versatile applicability and reusability of MCO-0.2

To investigate the universal applicability of MCO-0.2, THIA degradation in the MCO-0.2/PMS system were examined under different reaction conditions (*e.g.*, initial pH, PMS dosage, THIA concentration and co-existing anions). Fig. 4a showed the activity of MCO-0.2 was susceptible to the changes of pH value. The neutral pH condition achieved a higher THIA removal efficiency, while either acidic conditions or alkaline condition achieved a relatively low THIA degradation. Specifically, THIA removal efficiency was increased from 67.9% to 94.4% in 15 min by increasing the initial pH from 3.0 to 7.0. While THIA removal efficiency significantly declined from 94.4% to 41.9% with the further increase of pH from 7.0 to 11.0. As reported, $pK_{a_1}$ and $pK_{a_2}$ of PMS were about 0 and 9.4, respectively, which indicated that the main form of PMS was $HSO_5^-$ under the acidic conditions and neutral conditions, while the main form was $SO_5^{2-}$ under alkaline conditions.[42,43] Zero potential of MCO-0.2 was 6.91 (Fig. S3), demonstrating that the catalyst surface was mainly positively charged under negatively charged under alkaline conditions. As a result, pH has significant impact on the adsorption and existence form of PMS, thus notably affecting PMS activation. In the acidic solution, $HSO_5^-$ and RS could be severely scavenged by excessive $H^+$, therefore hampering PMS activation and THIA degradation. Under alkaline conditions, the main form of PMS was $SO_5^{2-}$ under alkaline conditions, which could be more difficultly activated to produce RS than that one ($HSO_5^-$) under acidic condition and neutral condition. Furthermore, the electrostatic repulsion between the negatively charged catalyst and $SO_5^{2-}$ also greatly restrained the adsorption of PMS on the catalyst surface, thus future blocked PMS activation.

As for PMS dosage (Fig. 4b), the degradation efficiency of THIA was sharply enhanced as PMS dosage increased from 0.2 to 0.8 mM. However, the enhancement was negligible with PMS dosage further increasing. The optimal dosage of PMS was 0.8 mM with respect to practical cost. Apparently, more PMS could generate more ROS in the reaction system and accelerate THIA degradation. However, excessive PMS might quench the active radicals in the reaction system and deteriorate THIA degradation. Similar results were also reported by Li and Gong's groups.[44,45] Fig. 4d showed THIA removal efficiency decreased from 94.4% to 40.3% as the concentration of THIA increased from 20 to 120 mg L$^{-1}$, and the rate constants (Fig. S4b) decreased from 0.2835 to 0.04475 min$^{-1}$, which could be attributed to insufficient RS produced from constant PMS to pollutants. Notable, although the reaction rates were different with the higher initial concentration of THIA (80 mg L$^{-1}$ *vs.* 120 mg L$^{-1}$), the final removal amount ($C_0$–$C$) was almost the

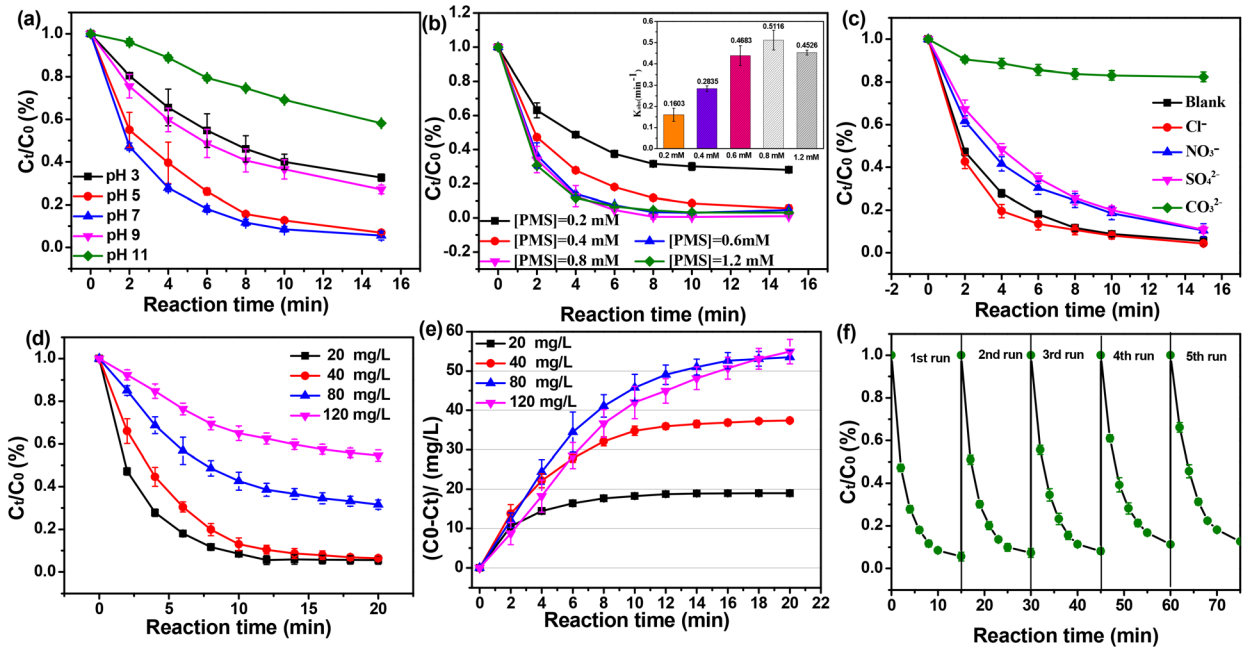


Fig. 4 Effects of (a) initial pH, (b) PMS concentration, (c) coexisting ions and (d) and (e) THIA concentration on THIA degradation in the MCO-0.2/PMS system; (f) THIA degradation in the recycle tests of MCO-0.2 catalysts. Reaction conditions: [THIA] = 20 mg L$^{-1}$, [PMS] = 0.4 mM, [catalyst] = 100 mg L$^{-1}$, $T$ = 298 K, pH = 7, $[Cl^-]_0 = [NO_3^-]_0 = [HCO_3^-]_0 = [SO_4^{2-}]_0$ = 100 mM.


© 2025 The Author(s). Published by the Royal Society of Chemistry

Open Access Article. Published on 28 August 2025. Downloaded on 2/6/2026 8:32:13 AM. This article is licensed under a Creative Commons Attribution 3.0 Unported Licence.

same (Fig. 4e), suggesting that the removal of one THIA might consumed approximately two PMS molecules for these concentrations.

Some anions (including $Cl^-$, $HCO_3^{2-}$, $NO_3^-$, and $SO_4^{2-}$) might be naturally present in actual water environment and affect THIA degradation.[46,47] Therefore, the impact of these co-existing anions on THIA degradation was investigated in the MCO-0.2/PMS process. As shown in Fig. 4c, $NO_3^-$ and $SO_4^{2-}$ possessed slight negative impact on THIA degradation with degradation efficiencies from 94.4% to 89.6% and 89.1% in 15 min, respectively, manifesting $NO_3^-$ and $SO_4^{2-}$ might react with reactive species ($SO_4^{\bullet-}$ and/or $^{\bullet}OH$) to generate the radicals with weaker redox, thus inhibit THIA degradation.[46] While THIA degradation efficiencies increased from 94.4% to 95.8% after $Cl^-$ was spiked the system, implying the reaction of $Cl^-$ and reactive species might convert into powerful radicals (such as $Cl_2^{\bullet-}$ and $ClO^{\bullet}$),[48] and future boost THIA degradation. Additionally, $HCO_3^-$ caused a significant restraint (https://fanyi.so.com/) on THIA removal with degradation efficiencies decline to 17.8% in 15 min, which might be attributed to the fact that $HCO_3^-$ could easily scavenge reactive species ($SO_4^{\bullet-}$ and/or $^{\bullet}OH$) $SO_4^{\bullet-}$ and/or $^{\bullet}OH$ to generate weak oxidant ($CO_3^{\bullet-}$), which attacks THIA more slowly.[49] THIA degradation in various water conditions (such as deionized water, tap water and lake water) was also investigated. As shown in Fig. S9, similar THIA removal rates were witnessed in deionized water (DI water) and tap water. In lake water, THIA removal rate exhibited an apparent inhibition but still exceeded 85%, suggesting excellent practical application prospects.

Finally, the reusability of MCO-0.2 catalysts was evaluated through successive THIA degradation tests. Fig. 4f showed that the degradation rates of THIA declined slightly and were still above 85% after five cycles. THIA degradation rate for the five recycles was 94.4%, 92.8%, 91.2, 88.8% and 87.3% in 15 min, and the rate constant ($k$) was estimated to be 0.2835, 0.2668, 0.2427, 0.2121 and 0.19297 $min^{-1}$ (Fig. S5b), demonstrating superior reusability of MCO-0.2. Simultaneously, the leaching of cobalt ion from MCO-0.2 catalysts was tracked during the successive processes. The dissolved cobalt ions for the five recycles was 0.082, 0.065, 0.062, 0.057 and 0.056 mg $L^{-1}$ (Fig. S5c), which were all far below the permissible discharge quantity for surface water in China.[3] In addition, THIA degradation was carried out in dissolved Co ions ($Co^{2+}$ 0.08 mg $L^{-1}$)/PMS system (Fig. S6) and THIA degradation efficiency was only 7.17%, indicating the leached cobalt ions contributed little to THIA removal. The above results prove MCO-0.2 catalysts have the excellent and stable catalytic activity just with a slight decrease after five cycles. The negligible decrease of the catalyst activity might be ascribed to the accumulation of products or intermediates on the catalyst during the THIA degradation process and cobalt leaching from the catalyst in the four recycling processes.

### 3.4 Mechanistic insights into PMS activation by MCO-0.2

**3.4.1 Identification of reactive species.** While it is generally agreed that various RS (including $SO_4^{\bullet-}$, $^{\bullet}OH$, $^1O_2$) were involved in the PMS-AOPs process, but their relative importance for pollutant abatement still remained significant controversies.[10] Originally, sulfate radical ($SO_4^{\bullet-}$) and its secondary radical (hydroxy radical, $^{\bullet}HO$) were proposed as the primary reactive intermediates for pollutant abatement during the persulfate-based process.[50–52] Recently, a series of increasing finding demonstrated that $^1O_2$ was the dominant reactive intermediates and played an even more important role than $SO_4^{\bullet-}$ and $^{\bullet}OH$ for pollutant abatement, especially during PMS-AOPs activated with carbon-based materials and carbon-metal composites.[53–55] However, latest studies[56,57] showed high-valent cobalt-oxo (Co(IV)=O) species were successfully detected in the PMS-AOPs by the fact that Co(IV)=O could easily oxidize DMSO to the corresponding sulfone product $PMSO_2$, and contributed greatly to pollutant abatement. Thus, it is crucial to delve deeper into the components of the MCO-0.2/PMS system, which dominated the reaction process.

First, quenching experiments were firstly conducted to prove the presence of ROS during the MCO-0.2/PMS process. MeOH was used as the scavengers of sulfate radical ($SO_4^{\bullet-}$) and hydroxy radical ($^{\bullet}HO$). While TBA, FFA and DMSO were applied to scavenge $^{\bullet}OH$, $^1O_2$ and Co(IV) =O, respectively. As reported, MeOH can synchronously scavenge $^{\bullet}OH$ or $SO_4^{\bullet-}$ ($k$(MeOH, $^{\bullet}OH$) = $9.7 \times 10^8$ $M^{-1}$ $s^{-1}$; $k$(MeOH, $SO_4^{\bullet-}$) = $3.2 \times 10^6$ $M^{-1}$ $s^{-1}$), but TBA can merely efficiently capture $^{\bullet}OH$ ($k$(TBA, $^{\bullet}OH$) = $6 \times 10^8$ $M^{-1}$ $s^{-1}$; and $k$(TBA, $SO_4^{\bullet-}$) = $8.4 \times 10^5$ $M^{-1}$ $s^{-1}$).[58] Fig. 5a and b showed TBA and MeOH could apparently inhibited THIA degradation and the degradation rate decreased from 94.3% to 81.21% and 48.21% in 15 min, respectively, confirming the generation of $SO_4^{\bullet-}$ and $^{\bullet}HO$ in THIA degradation. While FFA could almost completely inhibited THIA degradation, and the corresponding rate constant ($k$) decreased to 0.0122, accounting for a 95.69% decrease, which confirmed the generation of $^1O_2$ radicals. Further, the introduction of DMSO displayed a remarkably promoted inhibition for THIA degradation, and reduced the reaction rate by 63.76%. However, the formation of $PMSO_2$ could not catch in the process. Since the reaction of PMSO with $^{\bullet}OH$ or $SO_4^{\bullet-}$ could also result in a vigorous inhibitory for THIA abatement without the formation of $PMSO_2$,[59] it is reasonable to speculate that Co(IV)=O was almost absent in the reaction system.

Furthermore, EPR tests were performed to verify the formation of the above-mentioned ROS in MCO-0.2/PMS system. Fig. 5c and d showed no distinct characteristic peaks were detected when only PMS was introduced in the THIA solution, indicating that the generation of ROS from PMS self-decomposition was negligible. However, when PMS and MCO-0.2 were added simultaneously in the system, characteristic peaks of different ROS could be clearly observed. To be specific, Fig. 5c showed the four well-defined peaks with intensity ratio of 1 : 2 : 2 : 1 were ascribed to the characteristic signals of DMPO-$^{\bullet}OH$ adducts, while the rest peaks were accordant with typical character signals of DMPO-$SO_4^{\bullet-}$ adducts, signifying the formation of $^{\bullet}OH$ and $SO_4^{\bullet-}$ during the MCO-0.2/PMS process. In Fig. 5d, the three-line signals with an intensity ratio of 1 : 1 : 1 were observed, ascribing to the characteristic signals of $^1O_2$, confirmed the presence of $^1O_2$ in the THIA degradation process.

Open Access Article. Published on 28 August 2025. Downloaded on 2/6/2026 8:32:13 AM.
This article is licensed under a Creative Commons Attribution 3.0 Unported Licence.

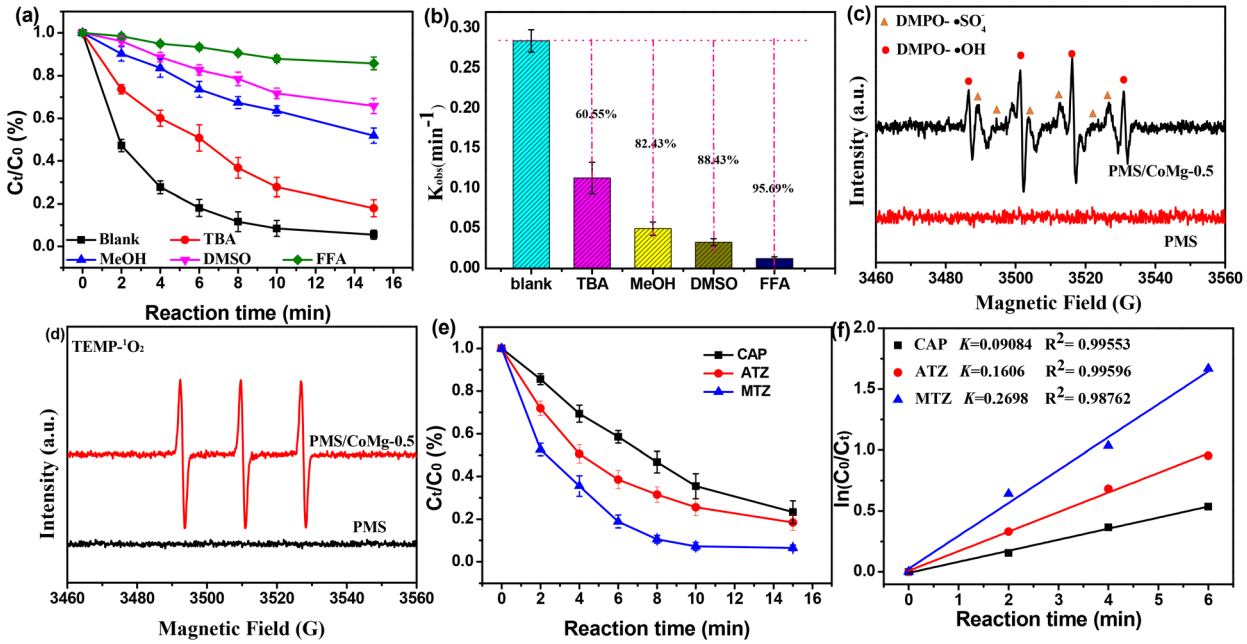


Fig. 5 (a) Removal efficiencies of THIA on MCO-0.2 catalysts in the presence of 200 mM quenchers, and (b) the corresponding first-order rate constants; EPR spectra of (c) DMPO and (d) TEMP as the trapping agent in the MCO-0.2/PMS system; (e) abatement of probe compounds on MCO-0.2 catalysts, and (f) the corresponding kinetic curves. Reaction conditions: [catalysts] = 100 mg $L^{-1}$, [PMS] = 0.4 mM, [THIA] = 20 mg $L^{-1}$, [CAP] = [ATZ] = [MTZ] = 0.08 mM, pH = 7, $T$ = 298 K.

Therefore, EPR measurement further identified the involvement of $^{\bullet}OH$, $SO_4^{\bullet-}$ and $^1O_2$ in THIA degradation, agreeing well with the results of quenching tests.

**3.4.2. Relative contributions of various reactive species.** The above results proved that $SO_4^{\bullet-}$, $HO^{\bullet}$ and $^1O_2$ were the reactive oxidants in the MCO-0.2/PMS system. Therefore, THIA degradation kinetic in the system could be simulated as follows:[60]

$$-\frac{d[THIA]}{dt} = k_{THIA}[THIA] \quad (3)$$

Integrating eqn (3) and yields eqn (4).

$$-\ln\frac{[THIA]}{[THIA]_0} = k_{THIA}t \quad (4)$$

$$k_{THIA} = k_{SO_4^{\bullet-}}[SO_4^{\bullet-}] + k_{\cdot OH}[^{\bullet}OH]_{ss} + k_{^1O_2}[^1O_2]_{ss} \quad (5)$$

where $[THIA]_0$ and $[THIA]$ were the concentration of THIA at time 0 and $t$, respectively. $k_{SO_4^{\bullet-},THIA}$, $k^{\bullet}_{OH,THIA}$ and $k_{^1O_2,THIA}$ were the second-order rate constant for the reaction of THIA with $SO_4^{\bullet-}$, $HO^{\bullet}$ and $^1O_2$, respectively (Table S2). $k_{THIA}$ was the pseudo-first-order rate constant of THIA degradation in the MCO-0.2/PMS system. $[SO_4^{\bullet-}]_{ss}$, $[^{\bullet}OH]_{ss}$ and $[^1O_{2ss}]$ represented the steady-state concentrations of $SO_4^{\bullet-}$, $HO^{\bullet}$ and $^1O_2$, respectively, and could be measured by several probe experiments.

In the probe experiments, probe compounds (including CAP, ATZ and MTZ) were added in the MCO-0.2/PMS system under identical conditions, and the abatement kinetic of these probes could be expressed as follows:

$$k_{CAP} = k_{SO_4^{\bullet-},CAP}[SO_4^{\bullet-}]_{ss} + k_{\cdot OH,CAP}[^{\bullet}OH]_{ss} + k_{^1O_2,CAP}[^1O_2]_{ss} \quad (6)$$

$$k_{ATZ} = k_{SO_4^{\bullet-},ATZ}[SO_4^{\bullet-}]_{ss} + k_{\cdot OH,ATZ}[^{\bullet}OH]_{ss} + k_{^1O_2,ATZ}[^1O_2]_{ss} \quad (7)$$

$$k_{MTZ} = k_{SO_4^{\bullet-},MTZ}[SO_4^{\bullet-}]_{ss} + k_{\cdot OH,MTZ}[^{\bullet}OH]_{ss} + k_{^1O_2,MTZ}[^1O_2]_{ss} \quad (8)$$

where $k_{CAP}$, $k_{ATZ}$ and $k_{MTZ}$ were the pseudo-first-order rate constants of the degradation of CAP, ATZ and MTZ probes in the MCO-0.2/PMS system, respectively, which were obtained from the kinetic plots in Fig. 5e and f. Moreover, $k_{SO_4^{\bullet-},CAP}$, $k^{\bullet}_{OH,CAP}$, $k_{^1O_2,CAP}$, $k_{SO_4^{\bullet-},ATZ}$, $k^{\bullet}_{OH,ATZ}$, $k_{^1O_2,ATZ}$, $k_{SO_4^{\bullet-},MTZ}$, $k^{\bullet}_{OH,MTZ}$ and $k_{^1O_2,ATZ}$ represented the second-order reaction rate constants of $SO_4^{\bullet-}$, $HO^{\bullet}$ and $^1O_2$ with CAP, ATZ and MTZ, respectively (Table S1). By using the eqn (6)–(8), the steady-state concentrations of $^1O_2$, $^{\bullet}OH$ and $SO_4^{\bullet-}$ in the MCO-0.2/PMS system were thus readily calculated to be $2.321 \times 10^{-10}$, $1.079 \times 10^{-11}$ and $4.408 \times 10^{-11}$ M, respectively.

Further, the relative contributions of $SO_4^{\bullet-}$, $HO^{\bullet}$, $^1O_2$ and other potential reactive species were defined as the ratios of THIA degradation rate induced by one specific reactive intermediate to the total degradation rate of THIA ($k_{THIA}$),[16] and could be expressed as follows:

$$R_{SO_4^{\bullet-}} = \frac{k_{SO_4^{\bullet-},THIA}[SO_4^{\bullet-}]_{ss}}{k_{SO_4^{\bullet-},THIA}[SO_4^{\bullet-}]_{ss} + k_{\cdot OH,THIA}[^{\bullet}OH]_{ss} + k_{^1O_2,THIA}[^1O_2]_{ss}} \quad (9)$$


© 2025 The Author(s). Published by the Royal Society of Chemistry

$$R_{\cdot OH} = \frac{k_{\cdot OH,THIA}[^{\cdot}OH]_{ss}}{k_{SO_4^{\cdot-},THIA}[SO_4^{\cdot-}]_{ss} + k_{\cdot OH,THIA}[^{\cdot}OH]_{ss} + k_{^1O_2,THIA}[^1O_2]_{ss}} \quad (10)$$

$$R_{^1O_2} = \frac{k_{^1O_2,THIA}[^1O_2]_{ss}}{k_{SO_4^{\cdot-},THIA}[SO_4^{\cdot-}]_{ss} + k_{\cdot OH,THIA}[^{\cdot}OH]_{ss} + k_{^1O_2,THIA}[^1O_2]_{ss}} \quad (11)$$

$$R_{other} = 1 - R_{SO_4^{\cdot-}} - R_{\cdot OH} - R_{^1O_2} \quad (12)$$

Using the newly measured kinetic data and the eqn (6)–(8), the relative contributions of $SO_4^{\cdot-}$, $HO^{\cdot}$, $^1O_2$ and other potential reactive species for THIA degradation in the MCO-0.2/PMS system were quantified to be 17.2%, 74.1%, and 3.5%, respectively. The measured results implied the contribution of $^{\cdot}OH$, $SO_4^{\cdot-}$ and $^1O_2$ to THIA abatement relied on both their reactivity and exposures. As reported,[61] $k_{SO_4^{\cdot-},THIA}$ and $k_{\cdot OH,THIA}$ were several orders of magnitude larger than $k_{^1O_2,THIA}$. Therefore, although the exposures of $^{\cdot}OH/^{\cdot}SO_4^{-}$ are about two or more times lower than that of $^1O_2$, they dominated THIA abatement in the system. Further, since $^{\cdot}OH$ exposures are 2.9 times higher than the exposures of $SO_4^{\cdot-}$, it contributed predominantly to THIA abatement in the MCO-0.2/PMS system given the similar value of $k_{SO_4^{\cdot-},THIA}$ and $k_{\cdot OH,THIA}$.

Combined with the above analysis, a possible activation mechanism of PMS on MCO-0.2 catalysts was proposed (Fig. S8). Initially, PMS was adsorbed onto the catalyst surface and activated by the active $Co^{2+}$, accompanying with the generation of $Co^{3+}$ and $SO_4^{\cdot-}$; meanwhile $Co^{3+}$ ions withdraw electrons from PMS to form $Co^{2+}$ and $SO_5^{\cdot-}$, driving a $Co^{2+}/Co^{3+}$ cycle. Subsequently, partial $SO_4^{\cdot-}$ further react with $H_2O$ or $OH^-$ of the solution to produce $HO^{\cdot}$. $SO_4^{\cdot-}$ and $HO^{\cdot}$ would also react with PMS to produce $SO_5^{\cdot-}$, which could be decomposed into $^1O_2$. Consequently, upon a rapid $Co^{2+}/Co^{3+}$ cycle, these generated RS could efficiently degraded THIA molecules over MCO-0.2 catalysts, where $HO^{\cdot}$ might contributed mainly to THIA degradation given the exposures of these RS and their reactivity with THIA.

## 4. Conclusions

Mg-doped $Co_3O_4$ with the regulated ratios of $Co^{2+}/Co^{3+}$ were prepared by incorporating Mg dopants into the lattice of $Co_3O_4$ and used as PMS activator for THIA degradation. Structural characterizations and experimental investigations confirmed that Mg doping did not change the $Co_3O_4$ host lattice and particle morphology, but could manipulate surface metal state of $Co_3O_4$ for an improved PMS activation. The optimized sample (MCO-0.2) with the suitable $Co^{2+}/Co^{3+}$ atomic ratios (1.13) exhibited efficient THIA degradation, and the rates constants (0.28347 $min^{-1}$) highly outperformed that of pure $Co_3O_4$, β-$Co(OH)_2$ and $ZnCo_2O_4$. A systematic analysis of the influences of reaction parameters indicated that the maximum degradation might be achieved under the conditions: catalyst dose 100 mg $L^{-1}$, PMS concentration 0.8 mM, pH 7 and THIA concentration 20 mg $L^{-1}$. Quenching experiment and ERP tests confirmed that $^1O_2$, $SO_4^{\cdot-}$ and $^{\cdot}OH$ were all involved in MCO-0.2/PMS System. According to a kinetic model and a series of probe compound-based experiments, the steady-state concentrations of $SO_4^{\cdot-}$, $HO^{\cdot}$ and $^1O_2$ were determined to be 1.079 × $10^{-11}$, 4.408 × $10^{-11}$ and 2.321 × $10^{-10}$ M in MCO-0.2/PMS system, and their corresponding contributions to THIA degradation were also quantified to 17.2%, 74.1%, and 3.5%. This work may inform a new approach for constructing efficient Fenton-like catalysis.

## Conflicts of interest

There are no conflicts to declare.

## Data availability

All data included in this study are available upon request by contact with the corresponding author.

Additional details on analytical methods of PMS and various organic pollutants, SI degradation results and the parameters for various organic pollutants, and other associated SI tables and figures. See DOI: https://doi.org/10.1039/d5ra04080a.

## Acknowledgements

This work was supported by Hubei Key Laboratory of Animal Nutrition and Feed Science, Wuhan Polytechnic University (No. 201911), the building project of Hubei Province for Technology Innovation and Entrepreneurship Service Capacity (No. 2018BEC466).

## Notes and references

1 A. Alsbaiee, B. J. Smith, L. L. Xiao, Y. H. Ling, D. E. Hebling and W. R. Dichtel, Rapid removal of organic micropollutants from water by a porous beta-cyclodextrin polymer, *Nature*, 2016, **529**, 190–194.
2 S. D. Richardson and T. A. Ternes, Water analysis: emerging contaminants and current issues, *Anal. Chem.*, 2014, **86**, 2813–2848.
3 Y. L. Luo, W. S. Guo, H. H. Ngo, L. D. Nghiem, F. I. Hai, J. Zhang, S. Liang and X. C. Wang, A review on the occurrence of micropollutants in the aquatic environment and their fate and removal during wastewater treatment, *Sci. Total Environ.*, 2014, **473–474**, 619.
4 M. S. Han, W. K. Zhu, M. S. A. Hossain, J. You and J. Kim, Recent progress of functional metal-organic framework materials for water treatment using sulfate radicals, *Environ. Res.*, 2022, **211**, 112956.
5 X. Wang, Z. Xiong, H. Shi, Z. Wu, B. Huang, H. Zhang, P. Zhou, Z. Pan, W. Liu and B. Lai, Switching the reaction mechanisms and pollutant degradation routes through active center size-dependent Fenton-like catalysis, *Appl. Catal., B*, 2023, **329**, 122569.
6 S. Mao, G. Y. Yao, P. Liu, C. Liu, Y. Wu, Z. T. Ding, C. Ding, M. Z. Xia and F. Y. Wang, Construction of an enhanced built-

Open Access Article. Published on 28 August 2025. Downloaded on 2/6/2026 8:32:13 AM. This article is licensed under a Creative Commons Attribution 3.0 Unported Licence.

Open Access Article. Published on 28 August 2025. Downloaded on 2/6/2026 8:32:13 AM. This article is licensed under a Creative Commons Attribution 3.0 Unported Licence.

in electric field in S-doped g-$C_3N_4$/$NiCo_2O_4$ for boosting peroxymonosulfate activation, *Chem. Eng. J.*, 2023, **470**, 144250.

7 Y. Bao, C. Lian, K. Huang, H. R. Yu, W. Y. liu, J. L. Zhang and M. Y. Xing, Generating High-valent Iron-oxo≡$Fe^{IV}$=O Complexes in Neutral Microenvironments through Peroxymonosulfate Activation by Zn-Fe Layered Double Hydroxides, *Angew. Chem., Int. Ed.*, 2022, **61**, e202209542.

8 C. L. Song, Q. Zhan, F. Liu, C. Wang, H. C. Li, X. Wang, X. F. Guo, Y. C. Cheng, W. Sun, L. Wang, J. S. Qian and B. C. Pan, Overturned loading of inert $CeO_2$ to active $Co_3O_4$ for unusually improved catalytic activity in Fenton-like reactions, *Angew. Chem., Int. Ed.*, 2022, **61**, e202200406.

9 J. Wang and S. Wang, Activation of persulfate (PS) and peroxymonosulfate (PMS) and application for the degradation of emerging contaminants, *Chem. Eng. J.*, 2018, **334**, 1502–1517.

10 Y. K. Pan, J. Z. Cao, M. Y Xing and Y. Y. Zhang, Current mechanism of peroxymonosulfate activation by cobalt-based heterogeneous catalysts in degrading organic compounds, *ACS ES&T Eng.*, 2024, **4**, 19–46.

11 J. Xie, S. H. Wu, C. Y. Luo, J. C. Zou, Y. Lin, S. Y. He and C. P. Yang, Modulating electronic structure of active sites on iron-based nanoparticles enhances peroxymonosulfate activation, *Appl. Catal., B*, 2024, **354**, 124138.

12 F. Li, Z. Lu, T. Li, P. Zhang and C. Hu, Origin of the Excellent Activity and Selectivity of a Single-Atom Copper Catalyst with Unsaturated Cu-$N_2$ Sites *via* Peroxydisulfate Activation: Cu(III) as a Dominant Oxidizing Species, *Environ. Sci. Technol.*, 2022, **56**(12), 8765–8775.

13 F. Wang, M. Xiao, X. Ma, S. Wu, M. Ge and X. Yu, Insights into the transformations of Mn species for peroxymonosulfate activation by tuning the $Mn_3O_4$ shapes, *Chem. Eng. J.*, 2021, **404**, 127097.

14 J. J. Jiang, Z. Q. Zhao, J. Y. Gao, T. R. Li, M. Y. Li, D. D. Zhou and S. S. Dong, Nitrogen Vacancy-Modulated Peroxymonosulfate Nonradical Activation for Organic Contaminant Removal *via* High-Valent Cobalt-Oxo Species, *Environ. Sci. Technol.*, 2022, **56**(9), 5611–5619.

15 J. J. Pei, K. X. Fu, Y. K. Fu, X. L. Liu, S. L. Luo, K. Yin and J. M. Luo, Manipulating High-Valent Cobalt-Oxo Generation on Co/N Codoped Carbon Beads *via* PMS Activation for Micropollutants Degradation, *ACS ES&T Eng.*, 2023, **3**(11), 1997–2007.

16 Y. L. Cao, Z. Wang, S. X. He, L. X. Shi, K. H. Guo and J. Y. Fang, Reinvestigation on High-Valent Cobalt for the Degradation of Micropollutants in the Co(II)/Peroxymonosulfate System: Roles of Co(III), *Environ. Sci. Technol.*, 2024, **58**(7), 3564–3575.

17 H. T. Li, Q. Gao, G. S. Wang, B. Han, K. S. Xia, J. P. Wu, C. G. Zhou and J. Dong, Postsynthetic incorporation of catalytically inert Al into $Co_3O_4$ for peroxymonosulfate activation and insight into the boosted catalytic performance, *Chem. Eng. J.*, 2021, **426**, 131292.

18 W. Li, S. Li, Y. Tang, X. Yang, W. Zhang, X. Zhang, H. Chai and Y. Huang, Highly efficient activation of peroxymonosulfate by cobalt sulfide hollow nanospheres for fast ciprofloxacin degradation, *J. Hazard. Mater.*, 2020, **389**, 121856.

19 H. Fui, S. M. Gao, X. R. Ma and Y. P. Huang, Facile fabrication of CoAl-LDH nanosheets for efficient rhodamine B degradation *via* peroxymonosulfate activation, *RSC Adv.*, 2023, **13**, 29695.

20 S. H. Wu, Z. W. Yang, Z. Y. Zhou, X. Li, Y. Lin, J. J. Cheng and C. P. Yang, Catalytic activity and reaction mechanisms of single-atom metals anchored on nitrogen-doped carbons for peroxymonosulfate activation, *J. Hazard. Mater.*, 2023, **459**, 132133.

21 J. Di, R. Jamakanga, Q. Chen, J. Li, X. Gai, Y. Li, R. Yang and Q. Ma, Degradation of rhodamine B by activation of peroxymonosulfate using $Co_3O_4$-rice husk ash composites, *Sci. Total Environ.*, 2021, **784**, 147258.

22 S. Shao, L. Qian, X. Zhan, M. Wang, K. Lu, J. Peng, D. Miao and S. Gao, Transformation and toxicity evolution of amlodipine mediated by cobalt ferrite activated peroxymonosulfate: effect of oxidant concentration, *Chem. Eng. J.*, 2020, **382**, 123005.

23 M. S. Wu, B. Xu and C. Y. Ouyang, Manipulation of spin–flip in $Co_3O_4$: a first principles study, *J. Mater. Sci.*, 2016, **51**, 4691–4696.

24 S. D. Liu, D. X. Ni, H. F. Li, K. N. Hui, C. Y. Ouyang and S. C. Jun, Effect of cation substitution on the pseudocapacitive performance of spinel cobaltite $MCo_2O_4$ (M = Mn, Ni, Cu, and Co) dagger, *J. Mater. Chem. A*, 2018, **6**, 10674–10685.

25 Y. Wei, J. Miao, J. Ge, J. Lang, C. Yu, L. Zhang, P. J. J. Alvarez and M. Long, Ultrahigh peroxymonosulfate utilization efficiency over CuO nanosheets *via* heterogeneous Cu(III) formation and preferential electron transfer during degradation of phenols, *Environ. Sci. Technol.*, 2022, **56**, 8984–8992.

26 J. Li, M. Xu, G. Yao and B. Lai, Enhancement of the degradation of atrazine through $CoFe_2O_4$ activated peroxymonosulfate (PMS) process: kinetic, degradation intermediates, and toxicity evaluation, *Chem. Eng. J.*, 2018, **348**, 1012–1024.

27 E. T. Yun, H. Y. Yoo, H. Bae, H. I. Kim and J. Lee, Exploring the role of persulfate in the activation process: radical precursor *versus* electron acceptor, *Environ. Sci. Technol.*, 2017, **51**, 10090–10099.

28 P. Niu, C. H. Li, D. Q. Wang, C. X. Jia, J. Zhao, Z. M. Liu, X. L. Zhang and L. L. Geng, Electronic modulation of fiber-shaped-$CoFe_2O_4$ *via* Mg doping for improved PMS activation and sustainable degradation of organic pollutants, *Appl. Surf. Sci.*, 2022, **605**, 154732.

29 X. P. Han, G. W. He, Y. He, J. F. Zhang, X. R. Zheng, L. L. Li, C. Zhong, W. B. Hu, Y. D. Deng and T. Y. Ma, Engineering Catalytic Active Sites on Cobalt Oxide Surface for Enhanced Oxygen Electrocatalysis, *Adv. Energy Mater.*, 2018, **8**, 1702222.

30 Q. F. Liu, Z. P. Chen, Z. Yan, Y. Wang, E. Wang, S. Wang, S. D. Wang and G. Q. Sun, Crystal-Plane-Dependent Activity of Spinel $Co_3O_4$ Towards Water Splitting and the


© 2025 The Author(s). Published by the Royal Society of Chemistry

Open Access Article. Published on 28 August 2025. Downloaded on 2/6/2026 8:32:13 AM. This article is licensed under a Creative Commons Attribution 3.0 Unported Licence.

Oxygen Reduction Reaction, *ChemElectroChem*, 2018, **5**, 1080–1086.

31 C. P. Plaisance and R. A. van Santen, Structure Sensitivity of the Oxygen Evolution Reaction Catalyzed by Cobalt(II,III) Oxide, *J. Am. Chem. Soc.*, 2015, **137**, 14660–14672.

32 X. Li, Z. Wang, B. Zhang, A. I. Rykov, M. A. Ahmed and J. Wang, $Fe_xCo_{3-x}O_4$ nanocages derived from nanoscale metal–organic frameworks for removal of bisphenol A by activation of peroxymonosulfate, *Appl. Catal., B*, 2016, **181**, 788–799.

33 M. Sun, S. N. Tang, Z. X. Chen, L. F. Zhai, Y. H. Xia and S. B. Wang, Mn-Doping-Induced $Co_3O_4$ Structural Distortion and Facet Change for Enhanced Electro-Activation of $O_2$ toward Pollutants Removal, *ACS ES&T Eng.*, 2024, **4**(8), 1970–1980.

34 Y. Xu, F. C. Zhang, T. Sheng, T. Ye, D. Yi, Y. J. Yang, S. J. Liu, X. Wang and J. N. Yao, Clarifying the controversial catalytic active sites of $Co_3O_4$ for the oxygen evolution reaction, *J. Mater. Chem. A*, 2019, **7**, 23191–23198.

35 P. Wu, L. Xia, Y. Liu, J. Wu, Q. Chen and S. Song, Simultaneous Sorption of Arsenate and Fluoride on Calcined Mg–Fe–La Hydrotalcite-Like Compound from Water, *ACS Sustain. Chem. Eng.*, 2018, **6**(12), 16287–16297.

36 A. F. Syeda and M. N. Khan, Spin State of Cobalt and Electrical Transport Mechanism in $MgCo_2O_4$ System, *J. Supercond. Novel Magn.*, 2018, **31**(11), 3545–3551.

37 W. Li, X. He, B. Li, B. Zhang, T. Liu, Y. Hu and J. Ma, Structural tuning of multishelled hollow microspheres for boosted peroxymonosulfate activation and selectivity: role of surface superoxide radical, *Appl. Catal., B*, 2022, **305**, 1210.

38 M. Li, S. You, X. Duan and Y. Liu, Selective formation of reactive oxygen species in peroxymonosulfate activation by metal-organic framework-derived membranes: a defect engineering-dependent study, *Appl. Catal., B*, 2022, **312**, 121419.

39 L. Zhuang, L. Ge, Y. Yang, M. Li, Y. Jia, X. Yao and Z. Zhu, Ultrathin iron-cobalt oxide nanosheets with abundant oxygen vacancies for the oxygen evolution reaction, *Adv. Mater.*, 2017, **29**(17), 1606793.

40 W. Zhang, S. Zhang, C. Meng and Z. Zhang, Nanoconfined catalytic membranes assembled by cobalt-functionalized graphitic carbon nitride nanosheets for rapid degradation of pollutants, *Appl. Catal., B*, 2023, **322**, 122098.

41 B. E. Channab, M. E. Ouardi, S. E. Marrane, O. A. Layachi, A. E. Idrissi, S. Farsad, D. Mazkad, A. BaQais, M. Lasri and H. A. Ahsaine, Alginate@$ZnCO_2O_4$ for efficient peroxymonosulfate activation towards effective rhodamine B degradation: optimization using response surface methodology, *RSC Adv.*, 2032, **13**, 20150–20163.

42 C. Tan, X. Lu, X. Cui, X. Jian, Z. Hu, Y. Dong, X. Liu, J. Huang and L. Deng, Novel activation of peroxymonosulfate by an easily recyclable VC@$Fe_3O_4$ nanoparticles for enhanced degradation of sulfadiazine, *Chem. Eng. J.*, 2019, **363**, 318–328.

43 H. Li, Q. Gao, G. Wang, B. Han, K. Xia and C. Zhou, Architecturing $CoTiO_3$ overlayer on nanosheets-assembled hierarchical $TiO_2$ nanospheres as a highly active and robust catalyst for peroxymonosulfate activation and metronidazole degradation, *Chem. Eng. J.*, 2020, **392**, 123819.

44 Z. Li, D. Liu, Y. Zhao, S. Li, X. Wei, F. Meng, W. Huang and Z. Lei, Singlet oxygen dominated peroxymonosulfate activation by CuO-$CeO_2$ for organic pollutants degradation: performance and mechanism, *Chemosphere*, 2019, **233**, 549–558.

45 C. Gong, F. Chen, Q. Yang, K. Luo, F. Yao, S. Wang, X. Wang, J. Wu, X. Li, D. Wang and G. Zeng, Heterogeneous activation of peroxymonosulfate by Fe-Co layered doubled hydroxide for efficient catalytic degradation of rhodamine B, *Chem. Eng. J.*, 2017, **321**, 222–232.

46 M. Murugalakshmi, K. Govindan, M. Umadevi, C. B. Breslin and V. Muthuraj, Fabrication of a $Sm_2O_3/In_2S_3$ photocatalyst for boosting ciprofloxacin oxidation and the Cr(VI) reduction: process parameters and degradation mechanism, *Environ. Sci.:Water Res. Technol.*, 2023, **9**, 1385–1402.

47 K. Govindan, D. G. Kim and S. O. Ko, Role of co-existing anions in non-radical and radical processes of carbocatalyzed persulfate activation for acetaminophen degradation, *Environ. Sci.:Water Res. Technol.*, 2022, **8**, 2940–2955.

48 R. D. Su, N. Li, Z. Liu, X. Y. Song, W. Liu, B. Y. Gao, W. Z. Zhou, Q. Y. Yue and Q. Li, Revealing the Generation of High-Valent Cobalt Species and Chlorine Dioxide in the $Co_3O_4$-Activated Chlorite Process: Insight into the Proton Enhancement Effect, *Environ. Sci. Technol.*, 2023, **57**(5), 1882–1893.

49 P. Devi, U. Das and A. Dalai, *In situ* chemical oxidation: principle and applications of peroxide and persulfate treatments in wastewater systems, *Sci. Total Environ.*, 2016, **571**, 643–657.

50 J. Wei, D. Han, J. Bi and J. Gong, Fe-doped ilmenite $CoTiO_3$ for antibiotic removal: electronic modulation and enhanced activation of peroxymonosulfate, *Chem. Eng. J.*, 2021, **423**, 130165.

51 L. Zhang, J. J. Qi, W. X. Chen, X. Y. Yang, Z. M. Fang, J. M. Li, X. Z. Li, S. Y. Lu and L. D. Wang, Constructing Hollow Multishelled Microreactors with a Nanoconfined Microenvironment for Ofloxacin Degradation through Peroxymonosulfate Activation: Evolution of High-Valence Cobalt-Oxo Species, *Environ. Sci. Technol.*, 2023, **57**(42), 16141–16151.

52 F. Li, Z. Lu, T. Li, P. Zhang and C. Hu, Origin of the Excellent Activity and Selectivity of a Single-Atom Copper Catalyst with Unsaturated Cu-$N_2$ Sites *via* Peroxydisulfate Activation: Cu(III) as a Dominant Oxidizing Species, *Environ. Sci. Technol.*, 2022, **56**(12), 8765–8775.

53 A. D. Bokare and W. Choi, Singlet-Oxygen Generation in Alkaline Periodate Solution, *Environ. Sci. Technol.*, 2015, **49**(24), 14392–14400.

54 Y. Wang, Y. Lin, S. Y. He, S. H. Wu and C. P. Yang, Singlet oxygen: properties, generation, detection, and environmental applications, *J. Hazard. Mater.*, 2024, **461**, 132538.

Open Access Article. Published on 28 August 2025. Downloaded on 2/6/2026 8:32:13 AM.
This article is licensed under a Creative Commons Attribution 3.0 Unported Licence.

55 L. Gao, Y. Guo, J. Huang, B. Wang, S. Deng, G. Yu and Y. Wang, Simulating micropollutant abatement during cobalt mediated peroxymonosulfate process by probe-based kinetic models, *Chem. Eng. J.*, 2022, **441**, 135970.

56 J. S. Song, N. N. Hou, X. C. Liu, M. Antonietti, Y. Wang and Y. Mu, Unsaturated single-atom $CoN_3$ sites for improved fenton-like reaction towards high-valent metal species, *Appl. Catal., B*, 2023, **325**, 122368.

57 Y. Zong, X. H. Guan, J. Xu, Y. Feng, Y. F. Mao, L. Q. Xu, H. Q. Chu and D. L. Wu, Unraveling the Overlooked Involvement of High-Valent Cobalt-Oxo Species Generated from the Cobalt(II)-Activated Peroxymonosulfate Process, *Environ. Sci. Technol.*, 2020, **54**(24), 16231–16239.

58 L. Gao, Y. Guo, J. Zhan, G. Yu and Y. Wang, Assessment of the validity of the quenching method for evaluating the role of reactive species in pollutant abatement during the persulfate-based process, *Water Res.*, 2022, **221**, 118730.

59 Z. Wang, J. Jiang, S. Pang, Y. Zhou, C. Guan, Y. Gao, J. Li, Y. Yang, W. Qiu and C. Jiang, Is Sulfate Radical Really Generated from Peroxydisulfate Activated by Iron(II) for Environmental Decontamination?, *Environ. Sci. Technol.*, 2018, **52**, 11276–11284.

60 H. J. Wang, L. W. Gao, Y. X. Xie, G. Yu and Y. J. Wang, Clarification of the role of singlet oxygen for pollutant abatement during persulfate-based advanced oxidation processes: $Co_3O_4$@CNTs activated peroxymonosulfate as an example, *Water Res.*, 2023, **244**, 120480.

61 G. Rózsa, L. Szabó, K. Schrantz, E. Takács and L. Wojnárovits, Mechanistic study on thiacloprid transformation: free radical reactions, *J. Photochem. Photobiol., A*, 2017, **343**, 17–25.


© 2025 The Author(s). Published by the Royal Society of Chemistry